Noncontact Human–Machine Interface With Planar Probing Coils in a Differential Sensing Architecture

Zhiming Xiao, *Member, IEEE*, Weibo Hu, Chenhui Liu, *Student Member, IEEE*, Hang Yu, and Changzhi Li, *Senior Member, IEEE*

***Abstract*— This paper presents a noncontact human–machine interface which is capable of sensing and indicating the position of a human hand that is approaching a probing coil. High sensitivity is achieved by utilizing a structure including two oscillators and a mixer to compare and extract the electromagnetic shift between two probing coils. The probing coils chosen in this system have a planar structure and small size, which can be easily built on a printed circuit board or integrated into a portable device for hand detection. The hand–coil interface is analyzed quantitatively for both the inductive and the capacitive links. Based on the analysis, a circuit model for the hand–coil interaction is presented. The proposed sensing circuit was built on an evaluation board with two commercial planar coils. A small phantom was used to imitate the hand electrical characteristic for a reliable and repeatable experimental setup. The measured results showed a hand-detection sensitivity of 10 kHz/mm at the output of the mixer stage and 30 mV/mm at the final output of the proposed interface.**

***Index Terms*— Bio-interaction, human–machine interface, sensitivity, sensor, wireless communication.**

I. Introduction

WIRELESS technologies have experienced significant advances over the past decades. They serve as the key technologies in many of today's daily routines, including personal communication, data transmission, and indoor/global positioning [1]. Most recently, both smart devices, such as laptops, PDAs, cell phones, and large appliances including thermostats, microwaves, and lighting management systems, have entered various aspects of human life as well. Thus, being able to wirelessly interact with users with a small probing coil or pad has become a competitive feature for those devices. For example, mechanical buttons or switches can be replaced by noncontact interface to enhance the device reliability and durability [2], [3]. Moreover, by integrating magnetic sensing coils in a glove [4], in a wireless power transfer coil [5], or in a smart phone [6], the human hand movement can be detected by those devices. Furthermore, by utilizing tiny probing pads and coils, human cardiorespiratory activity can also be monitored [7], [8]. While the potential of utilizing probing coils or pads in human-related or biorelated applications is promising, implementing an accurate and high sensitive interface is still challenging.

High sensitivity is hard to achieve because the electromagnetic field affected by human interaction only takes up a small portion of the original field, resulting in very limited electrical response [6]–[8]. In [6], a tiny frequency shift of ∼50 kHz was observed around a carrier frequency of 7 MHz while a hand was approaching a probing coil. In [7] and [8], to detect the biosignal with enough sensitivity, a microcontroller running at hundreds of megahertz was utilized to sense the tiny frequency shift, but the system complexity and cost were significantly increased.

To implement an accurate hand position detection is also challenging, due to below aspects. First, capacitive coupling [9] and inductive coupling [2], [10] are coexistent and affect the electrical response of the prober simultaneously. Second, the strength of both coupling links depends on the electrical characteristics of a human hand, such as the conductivity, the permeability, and the permittivity. Third, many other factors such as the distance, the orientation, and the gesture of the hand can affect the result as well. Therefore, the same electrical response may be caused by various possible conditions and an accurate positioning is not feasible through a single probing site. For instance, a hand at a closer distance may result in the same electrical response as that of a slightly higher conductive object at a farther distance.

The proposed human–machine interface is shown in Fig. 1. To improve the accuracy of detection, the human hand is sensed through multiple recording sites with a time-multiplexing scheme. This paper focuses on the design of the sensor with a fast enough speed that allows for the time-multiplexing function. To improve the detection sensitivity, a mixer is used in a differential structure to sense the electromagnetic shift between two recording sites. Each site uses a commercial planar coil that can be easily integrated into portable devices or large appliances.

This paper is organized as follows. The electromagnetic response of the hand–coil interference is analyzed in

Manuscript received July 11, 2017; revised September 27, 2017; accepted November 9, 2017. Date of publication February 13, 2018; date of current version March 8, 2018. This work was supported in part by the NSF under Grant ECCS-1254838 and Grant CNS-1718483 and in part by NSFC under Grant 61528104. The Associate Editor coordinating the review process was Dr. Sasan Bakhtiari. *(Corresponding author: Hang Yu.)*

Z. Xiao was with the Department of Electrical and Computer Engineering, University of Florida, Gainesville, FL 32603 USA. He is now with Linear Technology Corporation, Milpitas, CA 95035 USA (e-mail: xzm@ufl.edu).

W. Hu is with the Department of Electronic Information and Optical Engineering, Nankai University, Tianjin, China (e-mail: weibohu@hotmail.com).

C. Liu is with Qualcomm Inc., San Diego, CA 92121 USA (e-mail: chenhui.liu@ttu.edu).

H. Yu is with the College of Computer Science and Software Engineering, Shenzhen University, China (e-mail: yuhang@szu.edu.cn).

C. Li is with the Department of Electrical and Computer Engineering, Texas Tech University, TX 79424 USA (e-mail: changzhi.li@ttu.edu).

Color versions of one or more of the figures in this paper are available online at http://ieeexplore.ieee.org.

Digital Object Identifier 10.1109/TIM.2017.2784079

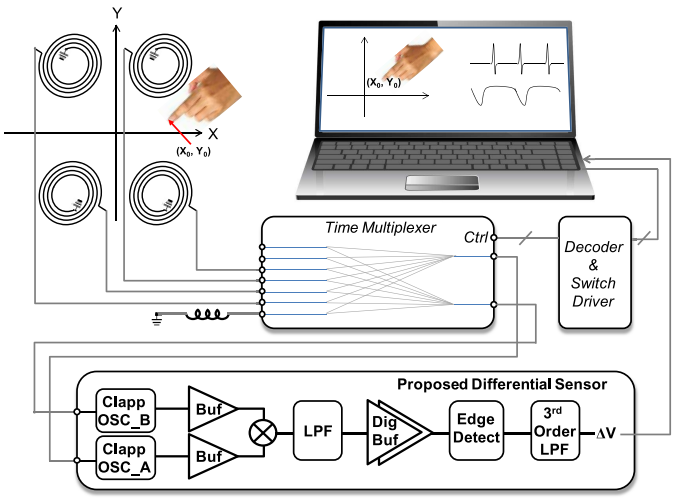

Fig. 1. Simplified system block diagram.

Section II. The circuit implementation of the proposed sensor is described in Section III. Then, the measurement results are discussed in Section IV, and a brief conclusion is drawn in Section V.

II. Coil–Hand Interface Model

Section II-A briefly describes the electromagnetic field in a planar coil. The magnetic and capacitive coupling effects are quantified in Sections II-B and II-C, respectively. The combined effects are modeled in Section II-D.

A. Electromagnetic Fields of a Coil

When a time-varying voltage is applied to a coil and induces a time-varying current, both electric and magnetic fields are established around the coil. Therefore, intrinsic parasitic capacitance always accompanies an inductor. If the coil is resonating with another capacitor, its oscillating frequency will be affected by the parasitic capacitance. As a result, when an object approaches the coil, due to different resistivities and dielectric constants of the object from the air, both fields, and thus the oscillating frequency will change. The coupling strength depends on various factors, such as the size, the orientation of the object, and the distance between the object and the coil [11].

The inductive link between the coil and the object can be modeled by a transformer with the object acting as its load [12]. A larger loading effect can be expected if the object has a lower resistivity which causes a larger secondary current in the transformer. The distance between the coil and the object is another factor that determines the strength of interference and sets the coupling coefficient (k) of the transformer. The induced current, known as the eddy current [13], [14], generates a magnetic field that counteracts the original magnetic field. The distribution and the density of the eddy current depend on the size and the resistivity of the object, as will be described in more detail in Section II-B.

The parasitic capacitance of the coil is related to its dimension, the core material, the shape of winding, and the permittivity of the insulator, etc. [15]. If an object is in proximity to the coil, the electric field will be affected due to its different dielectric constants from the air, which results in a change of the parasitic capacitance. A lumped capacitor model presented in [16] is derived for a single-layer coil wounded on a conductive core. This paper expands this idea and models the parasitic capacitance of a planar probing coil.

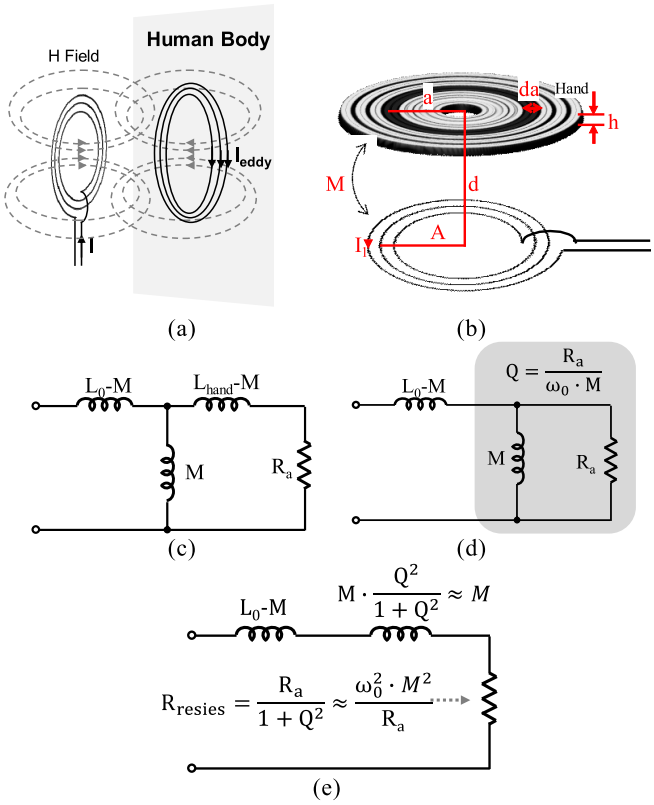

Fig. 2. Inductive link between a human body and a coil. (a) Magnetic coupling and induced eddy current. (b) Interaction between a coil and a human hand. (c) T-circuit model of the inductive link. (d) Simplified schematic in the case of $R_{\text{hand}} \gg \omega_0 \cdot (L_{\text{hand}} - \text{M})$. (e) Reformatted schematic after parallel-to-series transformation.

Both inductive and capacitive coupling will cause the impedance of the coil to change. An object that has high conductivity and large induced eddy current leads to a strong inductive coupling [7]. A coil that with a large number of turns and strong electric fields around shows an intensive capacitive coupling effect. This paper focuses on the analysis of a multiturn planar coil in the remaining of Section II for both the inductive and the capacitive coupling effects.

B. Inductive Coupling Effect

According to Faraday's Law, electromotive force is formed when an alternating magnetic flux is affecting a conductive material [17]. Therefore, an electromotive force and an induced eddy current will be formed inside a human hand when it approaches a coil in an oscillator, as shown in Fig. 2(a). The mutual inductance between the hand and the coil is denoted by M in Fig. 2(b). The inductive link can be modeled by a T-circuit with split inductors, as shown in Fig. 2(c) [12]. Since the resistance of the human hand is

much higher than the impedance of the split portion of the inductor ($R_{\text{hand}} \gg \omega_0 \cdot (L_{\text{hand}} - M)$), the secondary inductor can then be neglected for simplicity, as shown in Fig. 2(d). Using the parallel-to-serial conversion formula under high-Q (quality factor) condition, the inductive coupling model can be reformatted to the schematic shown in Fig. 2(e).

The distribution of the eddy current depends on the electric characteristic of the object that is in proximity of the coil. In one extreme case, if the object is a perfect conductor placed close enough, the induced eddy current will be distributed with a radius that is almost equal to the radius of the original current in the coil. This induced current is known as the image current [18]. In another extreme case, if the object has a relatively high impedance and the induced eddy current is much smaller than the one in the coil, the original magnetic field will be negligibly affected. In this case, the induced eddy current will distribute across all radii in the object and the currents at different radii hardly affect each other due to their small current values. This paper focus on the discussion of the second case due to the relatively large impedance of a human hand.

Based on the discussions earlier, this paper proposes a model that views the human hand as a combination of many coaxial rings which contribute to the inductive coupling effect independently, as shown in Fig. 2(b). Each ring has an eddy current flowing circularly and is analyzed independently. As a result, each ring acts as a parallel load to the T-circuit in Fig. 2(d) or a series load in Fig. 2(e). For the derivation consistency, the hand being sensed is assumed to be placed directly above the coil and its bottom surface is in parallel with the planar coil. The distance d between them is measured perpendicularly from the center of the coil to the hand, as shown in Fig. 2(b). The overall series resistance in Fig. 2(e) can then be calculated by integrating the resistance contributed by each coaxial ring across the radius

$$\begin{aligned} R_{\text{series},d} &= \int_0^b \frac{(\omega_0 \cdot N \cdot M_{a,d})^2}{R_a} da \\ &= \frac{h \cdot N^2 \cdot \omega_0^2}{2\pi\rho} \cdot \int_0^b f(a,d) da \end{aligned} \tag{1}$$

where ρ is the human hand resistivity, N is the number of turns of the coil, R_a is the resistance of the ring at a radius of a. The ring has a width of da and a thickness of h. The integration boundary b is the radius on the edge of a human hand. $M_{a,d}$ is the mutual inductance between the coil and the ring with a radius of a and a distance of d. The integrated term is denoted by $f(a,d)$, which is equal to $M_{a,d}^2/a$.

To obtain the mutual inductance between the coil and the hand, Maxwell's expression for mutual inductance of two coaxial circles placed close to each other can be used [19]

$$\begin{aligned} M_{a,d} &= \mu_0 a \left(\ln \frac{8a}{r} \left(1 + \frac{c}{2a} \cdots\right) - \left(2 + \frac{c}{2a} \cdots\right)\right) \quad a < A \\ M_{a,d} &= \mu_0 A \left(\ln \frac{8A}{r} \left(1 + \frac{c}{2A} \cdots\right) - \left(2 + \frac{c}{2A} \cdots\right)\right) \quad a > A \\ M_{A,d} &= \mu_0 A (\ln \frac{8A}{d} - 2) \quad a = A \end{aligned} \tag{2}$$

TABLE I
PARAMETERS OF THE HAND–COIL INTERFACE

Parameter	Value
Average radius of the planar coil, A	7.5 mm
Number of turns, N	30
Pitch of the turns, t	0.33 mm
Radius of the coil wire, r_0	0.15 mm
Original parasitic series resistance, R_{par}	0.4 Ω
Original inductance, L_0	12.3 μH
Original parasitic capacitance, $C_{parasitic}$	1.83 pF
Average hand thickness, h	15 mm
Average hand conductivity, ρ	2 Ω·m

where A is the average radius of the coil rings. The values of $c = |A - a|$ and $r = (c^2 + d^2)^{1/2}$ represent the radius difference and the shortest distance between the two rings, respectively. The term $f(a,d)$ can be reformatted as

$$\begin{aligned} f(a,d) &= \mu_0^2 a \left(\ln \frac{8a}{r} \left(1 + \frac{c}{2a} \cdots\right) - \left(2 + \frac{c}{2a} \cdots\right)\right)^2 \quad a < A \\ f(a,d) &= \frac{\mu_0^2 A^2}{a} \left(\ln \frac{8A}{r} \left(1 + \frac{c}{2A} \cdots\right) - \left(2 + \frac{c}{2A} \cdots\right)\right)^2 \quad a > A \\ f(A,d) &= \mu_0^2 A \left(\ln \frac{8A}{d} - 2\right)^2 \quad a = A. \end{aligned} \tag{3}$$

Since the integrated result of $R_{\text{series},d}$ in (1) represents the final series resistance in Fig. 2(e) caused by the hand interaction, the expression $f(a,d) \cdot da$ refers to a factor that is contributed to $R_{\text{series},d}$ by a ring with a radius of a, a distance of d and a width of da.

To quantify the inductive coupling effect, (3) is calculated based on the parameters of the interface listed in Table I. The calculated $f(a,d)$ as a function of the radius a at various distances d is plotted in Fig. 3(a). The peak value increases as the distance decreases, which infers that a stronger coupling happens at a shorter distance. To find out how $f(a,d)$ changes with the radius, the normalized value of $f(a,d)/\max(f(a,d))$ is plotted in Fig. 3(b). For a given distance d, the normalized value peaks near the radius of A, and drops as the radius increases or decreases. Therefore, the coupling effect by the hand regions with very large or small radius is negligible. The values of $\max(f(a,d))$ and $f(a,d)/\max(f(a,d))$ versus the hand–coil distance are plotted in Fig. 3(c). The result shows nearly a linear relationship between the integrated value and the distance, from which a slope can be extracted to approximate (1)

$$\begin{aligned} R_{\text{series},d} &= \frac{h \cdot N^2 \cdot \omega_0^2}{2\pi\rho} \cdot f(A,d) \cdot \int_0^b \frac{f(a,d)}{\max(f(a,d))} da \\ R_{\text{series},d} &\approx \frac{h \cdot N^2 \cdot \omega_0^2}{2\pi\rho} \cdot f(A,d) \cdot (2 + 2d). \end{aligned} \tag{4}$$

If the impedance of the coil is sensed by an LC resonating circuit, the oscillating frequency will shift when the hand approaches the coil. Assuming the LC tank has a capacitor C_0 of 22 pF (including the original parasitic capacitance of the coil $C_{\text{parasitic}}$) and all other parameters are listed in Table I,

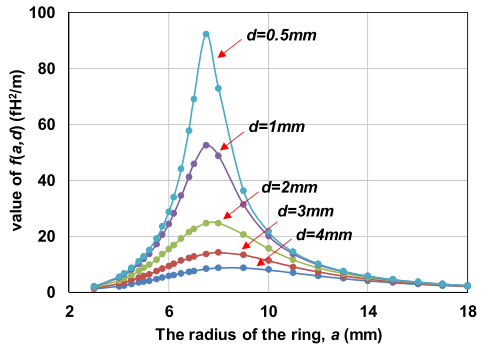

(a)

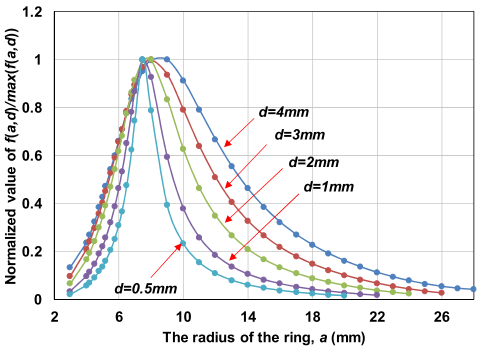

(b)

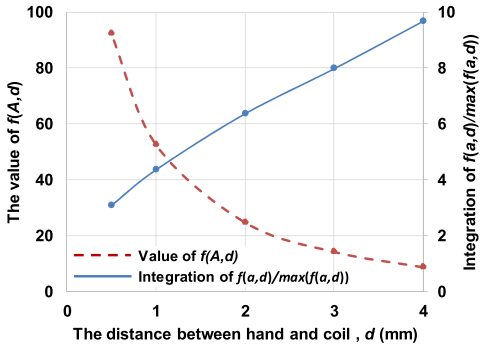

(c)

Fig. 3. Calculated inductive coupling effect of (a) $f(a,\ d)$ versus the radius of the ring. (b) Normalized value $f(a,\ d)/\max(f(a,\ d))$ versus the radius of the ring. (c) Value of $\max(f(a,\ d))$ and the integration of $f(a,\ d)/\max(f(a,\ d))$ versus the distance between hand and coil.

the resonant frequency including an induced series resistance $R_{\text{series},d}$ can be calculated based on [7] as

$$f_{\text{inductive},d} = \frac{1}{2\pi}\sqrt{\frac{1}{L_0 \cdot C_0} - \left(\frac{R_{\text{series},d}}{2L_0}\right)^2}. \tag{5}$$

The expression in (5) represents the resonant frequency due to hand interaction at a distance of d. By first-order Taylor series approximation, the frequency shift of $\Delta f_{\text{inductive},d} = (f_{\text{inductive},d} - f_0)$ can be simplified as

$$\Delta f_{\text{inductive},d} = -\frac{1}{8} f_0 \left(\frac{R_{\text{series},d}}{\sqrt{L_0/C_0}}\right)^2. \tag{6}$$

By inserting the integrated result of $f(a,d)/\max(f(a,d))$ into (4) and (6), the series resistance and the frequency shift versus the hand–coil distance can be calculated with the results plotted in Fig. 4. The solid portion of the curve is based on the

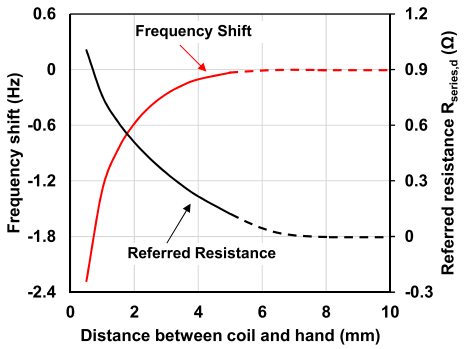

Fig. 4. Coupled series resistance and frequency shift as a function of the distance between a coil and a hand based on the inductive coupling model.

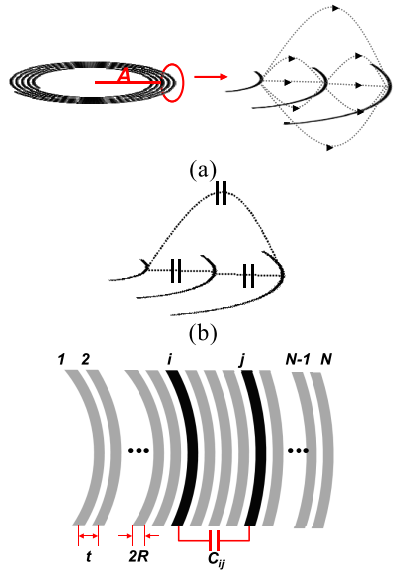

Fig. 5. Capacitive model of (a) electric field formed inside a coil, (b) intrinsic parasitic capacitor of the coil, and (c) capacitance between the ith and the jth turn.

calculation, whereas the dashed portion is estimated. This is because the mutual inductance equation (2) according to [19] is valid only when the hand–coil distance is relatively short compared with the coil radius.

C. Capacitive Coupling Effect

As shown in Fig. 5(a), electric fields are established among the turns of the coil which form the parasitic capacitors shown in Fig. 5(b). The coil windings are numbered as $1, 2, 3, \ldots N$, as shown in Fig. 5(c). For derivation simplicity, each winding is assumed to have an average radius of A, while the pitch between adjacent turns is t, and the diameter of the filament is $2R$. The capacitance between two parallel wires derived in [20] can be used to calculate the capacitance between the ith and the jth turns of the coil

$$C_{i,j} = \frac{\pi\,\varepsilon_0 \cdot 2\pi\,A}{\ln\left[\frac{t}{2r_0}(i-j) + \sqrt{\left(\frac{t}{2r_0}\right)^2 (i-j)^2 - 1}\right]}. \tag{7}$$

When a human hand approaches the ith and the jth turns of the coil as shown in Fig. 6(a), the affected and unaffected portions of the electric field are labeled as $C_{i,j,b}$ and $C_{i,j,a}$ with

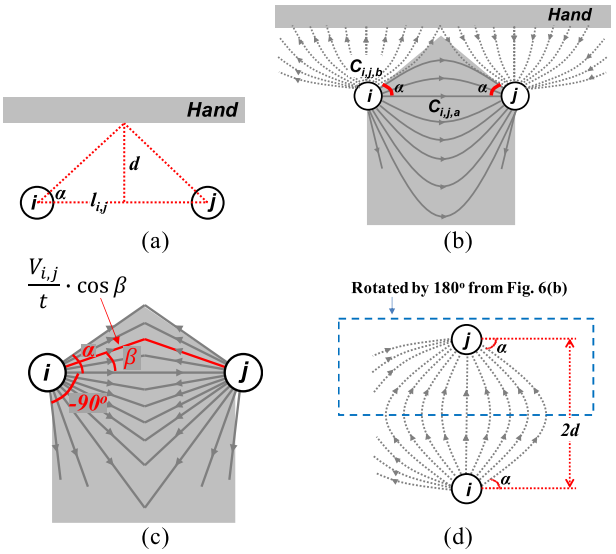

Fig. 6. Capacitive interference of the ith and jth turns of the coil. (a) Position between a hand and a coil. (b) Capacitance of unaffected and affected parts. (c) Electric field of unaffected and affected parts. (d) Equivalent electric field of the affected part.

unshaded and shaded mark in Fig. 6(b), respectively. Straight lines are used to approximate the electric field in Fig. 6(c). For a hand–coil distance of d, the angle between the coil plane and the center of the hand is labeled as α. For an arbitrary electric field line that has an angle of β to the coil plane, the electric field can be calculated as $V_{i,j}/t \cdot \cos\beta$, where $V_{i,j}$ is the voltage difference between the ith and jth turn. Then, the ratio between the unaffected capacitance and the original capacitance is

$$\frac{C_{i,j,a}}{C_{i,j}} \approx \frac{\int_{-\frac{\pi}{2}}^{\alpha} \frac{V_{i,j}}{l_{i,j}} \cdot \cos\beta \cdot d\beta}{\int_{-\frac{\pi}{2}}^{\frac{\pi}{2}} \frac{V_{i,j}}{l_{i,j}} \cdot \cos\beta \cdot d\beta} = \frac{\sin\alpha + 1}{2}$$
$$C_{i,j,a} \approx 0.5 \cdot C_{i,j} \cdot (\sin\alpha + 1) \tag{8}$$

where $C_{i,j}$ is the original unaffected capacitance between the ith and the jth turns. The capacitance $C_{i,j,b}$ represents the portion that the electric field is affected by the hand, shown as the dashed lines in the unshaded region of Fig. 6(b) and (d). Since the human hand has a much larger dielectric constant compared with the air, voltage drop inside the hand is negligible compared with the voltage drop outside the hand. As a result, the electric field of the affected region can be approximately by rotating the electric fields around the jth turn by 180° and placing it above the electric field generated by the ith turn, shown as the enclosed region of the dashed lines in Fig. 6(d) that is transferred from Fig. 6(b). The affected portion $C_{i,j,b}$ can then be calculated according to [20] as

$$C_{i,j,b} \approx 0.5 \cdot C_{i,j} \cdot (\cos\alpha + 1) \cdot p$$
$$p = \frac{\ln\left[\frac{t\cdot(i-j)}{2r_0} + \sqrt{\left(\frac{t\cdot(i-j)}{2r_0}\right)^2 - 1}\right]}{\ln\left[\frac{2d}{2r_0} + \sqrt{\left(\frac{2d}{2r_0}\right)^2 - 1}\right]} \tag{9}$$

where p refers to the ratio of the capacitance at a distance of $2d$ to the capacitance at a distance of $(i-j)\cdot t$.

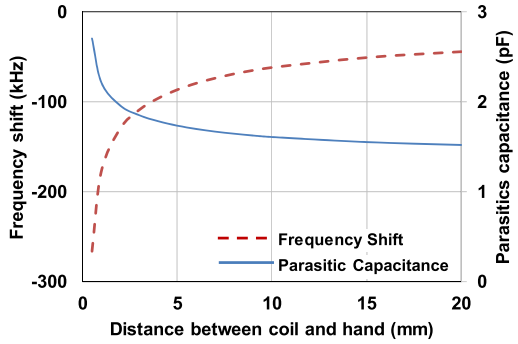

Fig. 7. Frequency shift and parasitic capacitance $C_{\text{parasitic},d}$ versus the distance between a coil and a hand by capacitive coupling.

By combining (8) and (9), the total capacitance between the ith and jth turns can be calculated as

$$C_{i,j,d} = C_{i,j,a} + C_{i,j,b} = 0.5 \cdot C_{i,j} \cdot (p \cdot \cos\alpha + \sin\alpha + p + 1)$$
$$\cos\alpha = \frac{(i-j)\cdot t}{\sqrt{4d^2 + (i-j)^2 t^2}}$$
$$\sin\alpha = \frac{2d}{\sqrt{4d^2 + (i-j)^2 t^2}}. \tag{10}$$

The result in (10) represents the capacitance between the ith and the jth turn with hand interference at a distance of d. The result can then be applied to calculate the overall capacitance of the coil with N turns to be

$$C_{\text{parasitic},d} = \sum_{i=2}^{N} \sum_{j=1}^{i-1} C_{i,j,d} \cdot \frac{(i-j)}{N}. \tag{11}$$

If the distance d goes to infinity, (11) turns out to be $C_{\text{parasitic}}$, which is the original unaffected parasitic capacitance of the coil ($C_{i,j}$). Assuming the coil parameters and the test conditions are the same as those for the inductive link in Table I, the parasitic capacitance of the coil as a function of the hand–coil distance can be calculated with results plotted in Fig. 7. As the distance decreases to below 5 mm, obvious capacitance change is resulted because more and more interwindings have significant portion of their electric fields affected by the hand. The frequency shift of $\Delta f_{\text{capacitive},d} = (f_{\text{capacitive},d} - f_0)$ due to the parasitic capacitive change of $\Delta C_{\text{parasitic},d} = (C_{\text{parasitic},d} - C_{\text{parasitic}})$ can be calculated as

$$\Delta f_{\text{capacitive},d} \approx \frac{f_0}{2} \cdot \frac{\Delta C_{\text{parasitic},d}}{C_0}. \tag{12}$$

The result of (12) is plotted in Fig. 7 which shows the frequency shift as a function of the hand–coil distance.

D. Combined Model for Both Capacitive and Inductive Links

The combined model that includes both the inductive and the capacitive coupling effects for the hand–coil interface is shown in Fig. 8. In this design, the LC resonant tank is implemented with a Clapp oscillator structure [19]. The free-running oscillating frequency (f_0) is set by L_0, and C_0 (including the original parasitic capacitance of the coil, $C_{\text{parasitic}}$). The inductive coupling results in an extra resistor in

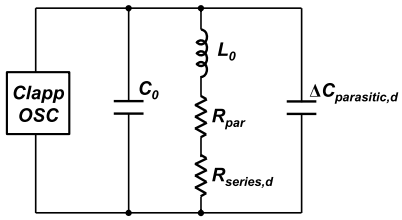

Fig. 8. Combined model of both inductive and capacitive links.

series with the coil, while the capacitive coupling results in an extra parasitic capacitor in parallel with the coil. The inductive and the capacitive couplings cause the oscillating frequency to shift high and low, respectively. The overall frequency shift of $\Delta f_d = (f_d - f_0)$ due to both coupling effects can be calculated with first-order approximation as

$$\Delta f_d = \Delta f_{\text{capacitive},d} + \Delta f_{\text{inductive},d}. \tag{13}$$

Based on the results from Sections III-B and III-C, the overall hand interference causes the frequency to shift low due to the dominance of capacitive coupling over the inductive coupling. This is because the human hand has a relative high resistivity and large relative permittivity. Moreover, the probing coil used in this paper is an off-the-shelf planar coil with a large number of turns, which has intensive electric field around and is affected by human hand. This conclusion can also be seen by comparing the results in Figs. 4 and 7.

The quality factor (Q) of the LC resonant tank in the combined model of Fig. 8 can therefore be calculated based on the results in Figs. 4 and 7. It shows that the quality factor drops as the hand approaches the coil but is still above 400 for a hand–coil distance larger than 0.5 mm, which satisfies the high-Q requirement for model derivation in Section II-B.

III. Circuit Implementation

The proposed sensor architecture is implemented by the circuits shown in Fig. 9. The front end consists of two Clapp oscillators [21] with two commercial planar coils, as shown in Fig. 9(a). The Clapp topology is chosen because its frequency can be tuned (by C_{TUNE}) without affecting the feedback capacitors (C_1 and C_2), and it shows better frequency stability compared with the Colpitts and the Hartley structure [22]. The coil has its parameters listed in Table I and serves as the probing coil in this paper. The nominal resonating frequency f_0 is set by the inductance of the probing coil L_0 and an effective capacitor C_0 with values determined by

$$C_0 = (1/C_1 + 1/C_2 + 1/C_3)^{-1} + C_{\text{TUNE}} + C_{\text{parasitic}} \tag{14}$$

where C_1 is used to block the dc current from the collector of Q_1 to the probing coil. The capacitors C_2 and C_1 form a negative feedback path in the loop with a common-base amplification stage by Q_1. The capacitive and inductive coupling effects through the hand–coil interface induce a parasitic capacitor $C_{\text{parasitic},d}$ and a series resistor $R_{\text{series},d}$, respectively. The capacitor C_{TUNE} is chosen to be a ceramic trimmer with an adjustable range of up to 10 pF. The oscillating frequency f_0 can thus be calculated to be 8 MHz. Based on

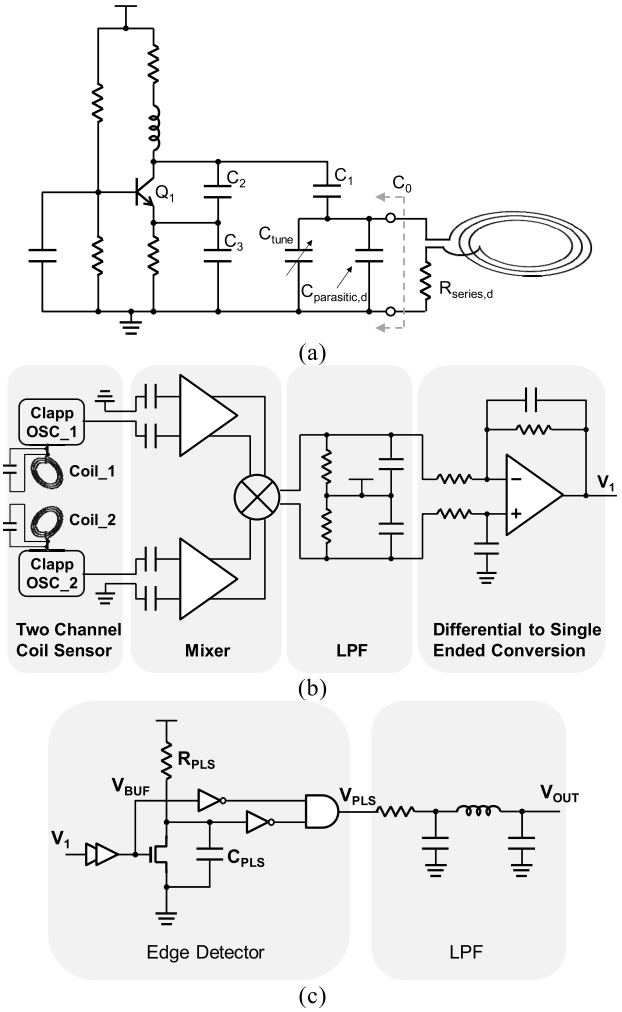

Fig. 9. Coil impedance sensing circuit. (a) Clapp oscillator. (b) Two channels with a differential structure and a mixer. (c) Frequency-to-voltage conversion circuit.

the calculated results in Fig. 7, the parasitic capacitance ($C_{\text{parasitic},d} - C_{\text{parasitic}}$) will change by 1–2 pF for hand–coil interaction within tens of mm, therefore C_{TUNE} is adjusted to give a C_0 value of 30 pF for enough frequency shift according to (12).

According to the results derived in Section II, the frequency shift caused by a hand interaction is about 100 kHz, which corresponds to a frequency change of around 1% of the carrier frequency at 8 MHz. In this paper, the 1% frequency shift is compared by a differential structure between the two input channels, as shown in Fig. 9(b). One channel serves as a reference clock to the other, and the frequency shift is down-converted by a mixer. In order to detect which coil is mainly interacting with the human hand, the two oscillators are tuned to have a preset offset frequency to each other, which is also the output frequency of the mixer. To be more specific, the offset is adjusted by fine-tuning C_{TUNE} so that OSC_1 resonates at a frequency that is 250 kHz higher than that of OSC_2. As a result, without hand interaction, the mixer output frequency is 250 kHz. If a hand is approaching Coil_1, the mixer output will decrease by tens to hundreds of kilohertz. Likewise, the mixer output frequency will increase if the

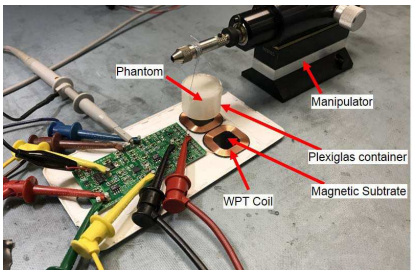

Fig. 10. Test bench of the proposed sensing circuit with a human body phantom.

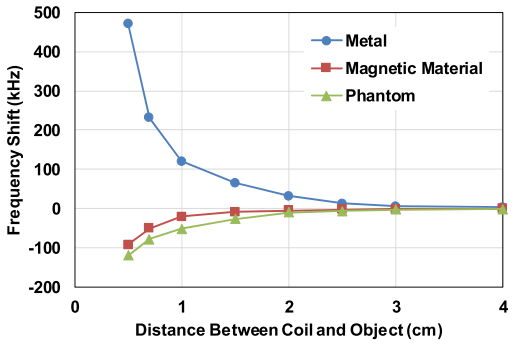

Fig. 11. Frequency shift as a function of the distance between the coil and three different materials.

hand approaches Coil_2. A low-pass filter is adopted after the mixer stage to remove the 8-MHz carrier and the high-frequency products of the mixer. The followed differential-to-single-ended conversion stage provides a low ripple output (V_1) with additional gain and a low-pass function.

Since the down-converted signal V_1 has a frequency shift of ∼30% around its center frequency for a hand–coil distance change of ∼10 mm, the frequency shift can be converted to an easy-to-read dc voltage shift by the schematic in Fig. 9(c). The filtered single-ended output V_1 is further buffered to form a rail-to-rail square wave V_{BUF} by several inverters. The edge detector circuit creates a pulse signal V_{PLS} at each falling edge of V_{BUF}. The pulsewidth (or the on-time) of the V_{PLS} is set by R_{PLS} and C_{PLS}, which create a delay on the rising edge of V_1. The pulsewidth is set to be around 0.8 μs, which yields a duty cycle change of around ±16% for a frequency shift of ±200 kHz. The third-order low-pass filter provides a low ripple dc voltage V_{OUT} that is proportional to the duty cycle of V_{PLS} and thus is also proportional to the frequency of V_1. For a 5-V supply voltage, V_{OUT} will have ±0.8 V voltage movement for a frequency shift of ±200 kHz on V_1. The speed that the proposed detector reacts to the hand movement is determined by the settling time of the third-order filter stage, which is around 0.5 ms and is fast enough to allow for a time-multiplexing function among multiple recording sites in Fig. 1.

In practical cases where the coil value suffers the nonideal factors such as variations and saturation effect, the accuracy of the frequency–distance relationship will degrade. However, the target resonance frequency of $(1/(L_0 \cdot C_0)^{1/2})$ can be trimmed to a fixed value by adjusting the C_{TUNE} value based on (14). Assuming the coil has inductance and parasitic capacitance tolerances of $\pm x\%$ and $\pm y\%$, respectively, the frequency shift due to the inductive coupling effect in (6) will remain almost the same, while the capacitive coupling effect in (12) will change by a factor of $(1\pm x\%)(1\pm y\%)$. Since the final filtered output voltage of the interface is proportional to the resonant frequency shift, the final dc output voltage will have a variation of $(1 \pm x\%)(1 \pm y\%)$ as well, considering the dominance of the capacitive coupling effect over inductive coupling effect.

IV. Experiment

The proposed differential sensor in Fig. 9 was built on an evaluation board with a size of ∼5 cm × 10 cm, as shown in Fig. 10(a). The two probing coils were chosen to be planar structure from TDK with parameters listed in Table I. The n-p-n transistor was chosen to be MMBT3904LT1G from On-Semi. The LTC5510 broadband mixer was selected to extract the frequency difference between the two Clapp oscillators. In order to establish a reliable and repeatable measurement setup, a human body phantom was used for imitating the human hand. The composition of the phantom was the same as that in [23], which can mimic the human body electrical characteristic at tens of MHz which is the resonate frequency of the Clapp oscillator in this design. The hand–coil distance was controlled by a manipulator as shown in Fig. 10(b). The object being sensed was placed right above the coil with its bottom plate in parallel to the planar coil plane. The hand–coil distance d was measured perpendicularly from the center of the coil to the object under test.

As shown in Fig. 11, the first experiment was carried out to check the frequency change caused by three different materials that have the same area on the bottom side: metal, magnetic material, and the human body phantom. The metal (copper) with a conductivity of 6×10^7 S/m resulted in a large internal eddy current, so the initial magnetic field was counteracted and the effective inductance was reduced. Therefore, when the piece of metal approached the coil, the oscillating frequency increased. The magnetic material (ferrite) [24] with a conductivity of 0.001 S/m and a relative permeability of ∼650 caused the inductance of the probing coil to increase and the oscillating frequency to decrease. The human body phantom [23] with a conductivity of 0.3 S/m, a relative permittivity of ∼500 and a relative permeability of ∼1 was held by a thin Plexiglas container and caused the oscillating frequency to decrease. The results from those example materials showed the possibility of the hand recognition by the proposed sensor but with a high requirement on the accuracy of detection. The proposed high-level system diagram in Fig. 1 with a probing coil array can improve the accuracy of hand identification by extracting information from multiple recording sites. However, a larger number of coils may result in higher cost and more stringent requirements on the sensor speed.

The measured waveforms at the output of the mixer stage and at the output of the filter stage under different hand–coil distance conditions are shown in Fig. 12. When the hand approached Coil_1 in Fig. 9(b), the frequency of OSC_1 decreased while the frequency of OSC_2 remained almost the same, so the mixed frequency decreased to ∼50 kHz and the final filtered V_{OUT} voltage was 5.2 V, as shown in Fig. 12(b). For the same reason, the mixed output

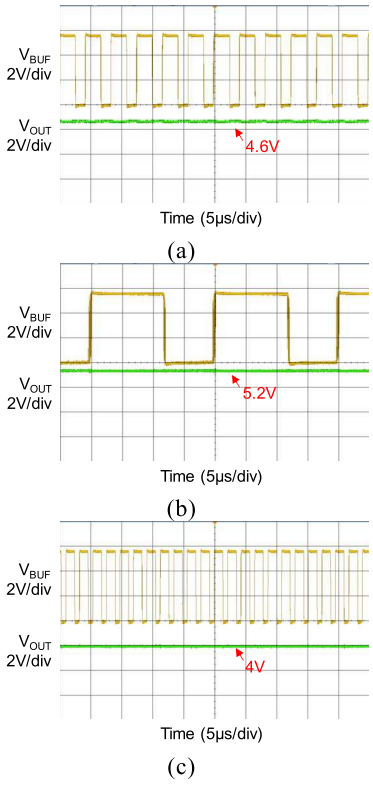

Fig. 12. Measured waveforms at the output of the digital buffer and the output of final filter stage (a) when hand was far away from both coils, (b) when hand approached Coil_1, and (c) when hand approached Coil_2.

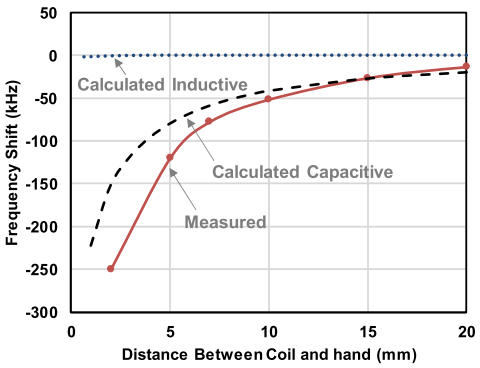

Fig. 13. Frequency shift versus the distance between the coil and the hand based on the capacitive and inductive models.

TABLE II
COMPARISON AMONG WIRELESS SENSORS

	[6] Liu	[7] Teichmann	[3] Steffen	[2] TI	This work
Year	2015	2013	2007	2015	2017
Application	Hand Sensing	Cardio-respiratory	Cardio-respiratory	Conductive target	Hand sensing
Coupling Method	Both	Both	Both	Inductive	Capacitive
Type of prober	Coil	Electrode	Electrode	Coil	Coil
Sensitivity	$\Delta f/f_0 \approx$ 0.07%*	$\Delta f/f_0 \approx$ 0.09%*	N/A	10 codes/mm*	$\Delta f/f_0$ $\approx$ 4%
Complexity	Not processed	Need μC	Need μP	Need Freq. counter	Need Mixer

* Extracted from measured results.

frequency increased to ∼450 kHz when the hand approached Coil_2 and the final filtered V_{OUT} voltage was measured to be 4 V, as shown in Fig. 12(c). The measured result shows a nonlinear relationship between the output voltage and the hand–coil distance, so a sensitivity is reported by averaging the results over a range of 2–20 mm. The result shows a sensitivity of ∼10 kHz/mm which corresponds to a frequency shift of 4% per mm around its carrier frequency of 250 kHz. At the final output stage of the proposed interface, the measured voltage sensitivity to the hand movement was 30 mV/mm. The result was much improved compared with the previous single-ended approach without a mixer incorporated [6], which had a sensitivity of 0.07% per mm around its carrier frequency of 7 MHz. However, the sensitivity was improved at the expense of increased cost and solution size, since extra components such as a Clapp oscillator, a mixer, and a coil are required.

The measured result is compared with the theoretical results calculated by the model in Section II, as shown in Fig. 13. The experiment was conducted by utilizing a human body phantom to imitate the electric characteristic of human hand for a repeatable and reliable setup. The theoretical results based on the model exhibited a good prediction of the measurement result. The deviation between the calculated and measured results is twofold. First, there are several approximations made while deriving the model. For example, straight lines were used to represent the electrical field, and the voltage drop of the electric field inside the hand was neglected. Second, the shape of the phantom has different parameters than the ones of a human hand in Table I. In an actual hand-detection application, however, reduced repeatability and more deviations are expected if other nonidealities are included, such as the orientation, the thickness, and the moisture level of a hand. Moreover, as discussed in Section III, hardware components of the proposed interface such as the coil and the capacitors have variations, which also affect the accuracy of the system. Therefore, the proposed human hand-detection approach exhibited high sensitivity but still needs future improvement for an accurate position calculation regarding the nonidealities mentioned earlier.

To compare the performance among the biosensing approaches, Table II lists some specifications from different designs. The proposed method that utilizes a mixer to extract the electromagnetic shift exhibits a much-improved detection sensitivity and reduced system complexity compared with the approaches with a counter [2] or a μP [3], [7].

V. CONCLUSION

This paper presented a human hand sensor with a planar probing coil, which is compatible with portable devices and large appliances. The inductive and capacitive model for the hand–coil interaction was derived to predict the impedance change of the coil by hand interference. The sensitivity of the proposed sensor was improved by utilizing a mixer in a differential structure that down-converts the frequency shift to baseband. The measured output showed a sensitivity

of 30 mV/mm to the hand movement, which can be easily processed by succeeding stages. The fast conversion speed of the proposed interface allows the sensor to be shared by multiple recording sites for improved detection accuracy.

REFERENCES

[1] S. Stoecklin, A. Yousaf, T. Volk, and L. Reindl, "Efficient wireless powering of biomedical sensor systems for multichannel brain implants," *IEEE Trans. Instrum. Meas.*, vol. 65, no. 4, pp. 754–764, Apr. 2015.

[2] *Inductance-to-Digital Converter*, Texas Instrum., Dallas, TX, USA, Sep. 2013.

[3] M. Steffen, A. Aleksandrowicz, and S. Leonhardt, "Mobile noncontact monitoring of heart and lung activity," *IEEE Trans. Biomed. Circuits Syst.*, vol. 1, no. 4, pp. 250–257, Dec. 2007.

[4] C.-S. Fahn and H. Sun, "Development of a data glove with reducing sensors based on magnetic induction," *IEEE Trans. Ind. Electron.*, vol. 52, no. 2, pp. 585–594, Apr. 2005.

[5] S. A. Mirbozorgi, H. Bahrami, M. Sawan, and B. Gosselin, "A smart multicoil inductively coupled array for wireless power transmission," *IEEE Trans. Ind. Electron.*, vol. 61, no. 11, pp. 6061–6070, Nov. 2014.

[6] C. Liu, C. Gu, and C. Li, "Non-contact hand interaction with smart phones using the wireless power transfer features," in *Proc. Radio Wireless Symp. (RWS)*, San Diego, CA, USA, Jan. 2015, pp. 20–22.

[7] D. Teichmann, J. Foussier, J. Jia, S. Leonhardt, and M. Walter, "Noncontact monitoring of cardiorespiratory activity by electromagnetic coupling," *IEEE Trans. Biomed. Eng.*, vol. 60, no. 8, pp. 2142–2152, Aug. 2013.

[8] D. Teichmann, D. De Matteis, T. Bartelt, M. Walter, and S. Leonhardt, "A bendable and wearable cardiorespiratory monitoring device fusing two noncontact sensor principles," *IEEE J. Biomed. Health Informat.*, vol. 19, no. 3, pp. 784–793, May 2015.

[9] S. Noopuran and P. Kaur, "Proximity sensing in mobile phones," Cypress Semicond., San Jose, CA, USA, Tech. Rep., Jan. 2014.

[10] V. J. Brusamarello, Y. B. Blauth, R. de Azambuja, I. Müller, and F. R. de Sousa, "Power transfer with an inductive link and wireless tuning," *IEEE Trans. Instrum. Meas.*, vol. 62, no. 5, pp. 924–931, May 2013.

[11] Z. Xiao, D. Genschow, C. Liu, Y. Li, and C. Li, "Non-contact human machine interface based on bio-interaction with wireless power transfer features," in *Proc. RF Wireless Technol. Biomed. Healthcare Appl. (IMWS-BIO)*, Taipei, Taiwan, Sep. 2015, pp. 167–168.

[12] D. Li *et al.*, "Wireless sensing system-on-chip for near-field monitoring of analog and switch quantities," *IEEE Trans. Ind. Electron.*, vol. 59, no. 2, pp. 1288–1299, Feb. 2011.

[13] X. Ma and A. J. Peyton, "Eddy current measurement of the electrical conductivity and porosity of metal foams," *IEEE Trans. Instrum. Meas.*, vol. 55, no. 2, pp. 570–576, Apr. 2006.

[14] H.-Y. Wei and A. J. Wilkinson, "Design of a sensor coil and measurement electronics for magnetic induction tomography," *IEEE Trans. Instrum. Meas.*, vol. 60, no. 12, pp. 3853–3859, Dec. 2011.

[15] S. W. Pasko, M. K. Kazimierczuk, and B. Grzesik, "Self-capacitance of coupled toroidal inductors for EMI filters," *IEEE Trans. Electromagn. Compat.*, vol. 57, no. 2, pp. 216–223, Apr. 2015.

[16] A. Massarini and M. K. Kazimierczuk, "Self-capacitance of inductors," *IEEE Trans. Power Electron.*, vol. 12, no. 4, pp. 671–676, Jul. 1997.

[17] E. C. Jordan and K. G. Balmain, *Electromagnetic Waves and Radiating Systems*. Tokyo, Japan: Prentice-Hall, 1968.

[18] M. Montrose, *Printed Circuit Board Basics*. Hoboken, NJ, USA: Wiley, 2000, pp. 13–63.

[19] E. B. Rosa and F. W. Grover, "Formulas and tables for the calculation of mutual and self inductance. (Revised.)," *J. Washington Acad. Sci.*, vol. 1, nos. 1–2, pp. 14–16, 1948.

[20] J. D. Jackson, *Classical Electrodynamics*. New York, NY, USA: Wiley, 1975, p. 80.

[21] J. K. Clapp, "An inductance-capacitance oscillator of unusual frequency stability," *Proc. IRE*, vol. 36, no. 3, pp. 356–358, Mar. 1948.

[22] B. R. Eisenberg, "Frequency stability of a Clapp VCO," *IEEE Trans. Instrum. Meas.*, vol. IM-18, no. 3, pp. 221–224, Sep. 1969.

[23] T. Yamamoto *et al.*, "Development of electromagnetic phantom at low-frequency band," in *Proc. IEEE EMBS*, Osaka, Japan, Jul. 2013, pp. 1887–1890.

[24] *Ferrite Plates for Wireless Charging_MP&33 Series*, Laird-Signal Integrity, Laird Smart Technol., Chesterfield, MO, USA, 2014.

Zhiming Xiao (M'17) received the B.S. degree from the Huazhong University of Science and Technology, Wuhan, China, in 2006, and the M.S. and Ph.D. degrees in electrical engineering from the University of Florida, Gainesville, FL, USA, in 2008 and 2013, respectively.

Since 2011, he has been a Design Engineer with the Analog Devices' Power Management IC Group, Milpitas, CA, USA. His current research interests include micropower analog circuits design, switching power converters, and their digital control techniques.

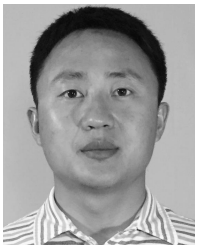

Weibo Hu received the bachelor's degree from the Harbin Institute of Technology, Harbin, China, in 2005, the master's degree from Peking University, Beijing, China, in 2008, and the Ph.D. degree from Texas Tech University, Lubbock, TX, USA, in 2014.

He was with the Mixed-Signal Department, Qualcomm Inc., San Diego, CA, USA, for four years. He was a Faculty Member with Nankai University, Tianjin, China, where he is currently a Professor with the Microelectronics Department. His current research interests include mixed-signal integrated circuits and system design. Besides designing some mixed-signal blocks, his lab tries to design circuits or systems to mimic human thinking and sensing, such as implementing artificial intelligence chips and small radar-based sensing systems.

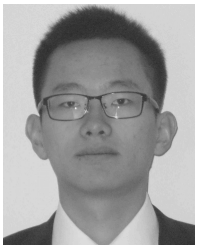

Chenhui Liu (S'15) received the B.S. degree in optoelectronic information engineering from the Huazhong University of Science and Technology, Wuhan, China, in 2013, and the M.S. degree in electrical engineering from Texas Tech University, Lubbock, TX, USA, in 2015.

He is currently an Applications Engineer with Qualcomm Inc., San Jose, CA, USA. His research interests include RF systems, RF transceivers, and the applications of RF/wireless technologies.

Hang Yu received the M.Sc. degree from the University of Massachusetts, Amherst, MA, USA, in 2004, and the Ph.D. degree from the University of Florida, Gainesville, FL, USA, in 2010.

He is currently an Associate Professor with the College of Computer Science and Software Engineering, Shenzhen University, Shenzhen, China. His current research interests include low-power RF/mixed-signal IC design, system-on-a-chip for biomedical applications, and miniature antenna design.

Changzhi Li (S'06–M'09–SM'13) received the B.S. degree in electrical engineering from Zhejiang University, Hangzhou, China, in 2004, and the Ph.D. degree in electrical engineering from the University of Florida, Gainesville, FL, USA, in 2009.

From 2007 to 2009, he was with Alereon Inc., Austin, TX, USA, and Coherent Logix Inc., Austin, TX, USA, where he was involved in ultra-wideband transceivers and software-defined radio. In 2009, he joined Texas Tech University, Lubbock, TX, USA, as an Assistant Professor, where he is currently an Associate Professor. His current research interests include the biomedical applications of microwave/RF, wireless sensor, and analog circuits.

Dr. Li was a recipient of the NSF Faculty Early CAREER Award in 2013, the ASEE Frederick Emmons Terman Award in 2014, and the IEEE-HKN Outstanding Young Professional Award in 2014. He is an Associate Editor of the IEEE TRANSACTIONS ON CIRCUITS AND SYSTEMS—I: REGULAR PAPERS and the IEEE JOURNAL OF ELECTROMAGNETICS, RF AND MICROWAVES IN MEDICINE AND BIOLOGY. He served as the TPC Co-Chair for the IEEE Wireless and Microwave Technology Conference in 2012 and 2013, and an Associate Editor for the IEEE TRANSACTIONS ON CIRCUITS AND SYSTEMS—II: EXPRESS BRIEFS in 2014 and 2015.